2013 IEEE 10th International Symposium on Biomedical Imaging:
From Nano to Macro
San Francisco, CA, USA, April 7-11, 2013

MODELING AIRWAY PROBABILITY

Rina D. Rudyanto[1], Arrate Muñoz-Barrutia[1], Alejandro A. Diaz[2], James Ross[2]
George R. Washko[2], Carlos Ortiz-de-Solorzano[1], Raul San Jose Estepar[2]

[1]Center for Applied Medical Research, University of Navarra, Pamplona, Spain
[2]Brigham and Women's Hospital, Boston, MA

ABSTRACT

We present a probability model for lung airways in computed tomography (CT) images. Lung airways are tubular structures that display specific features, such as low intensity and proximity to vessels and bronchial walls. From these features, the posterior probability for the airway feature space was computed using a Bayesian model based on 20 CT images from subjects with different degrees of Chronic Obstructive Pulmonary Disease (COPD). The likelihood probability was modeled using both a Gaussian distribution and a nonparametric kernel density estimation method. After exhaustive feature selection, good specificity and sensitivity were achieved in a cross-validation study for both the Gaussian (0.83, 0.87) and the nonparametric method (0.79, 0.89). The model generalizes well when trained using images from a late stage COPD group. This probability model may facilitate airway extraction and quantitative assessment of lung diseases, which is useful in many clinical and research settings.

Index Terms—CT, lung, probability model, airway segmentation, chronic obstructive pulmonary disease

1. INTRODUCTION

Chronic Obstructive Pulmonary Disease (COPD) is the third leading cause of death and disability in the world. COPD is characterized by progressive expiratory airflow obstruction, due to one or the combination of two phenotypes: emphysema and airway obstruction. The analysis of thoracic computed tomography (CT) images helps to better characterize COPD by studying anatomical remodeling due to tissue loss and changes in airway dimensions. This analysis relies on accurate segmentation of various structures in the lungs, such as airways and vessels, made challenging because of natural and pathological variability in size, curvature, orientation, and proximity to other organs.

Traditionally, airways in lung CT images have been associated with image features such as low attenuation image values – airways are filled with air-, surrounded by high attenuation circular or semi-circular shapes. To segment airways, the search space could typically encompass the volume of the entire lung. To limit the search space, prior knowledge of the lung anatomy can be used, for instance by starting the search from a point in the trachea, to detect the rest of the airway tree using region growing algorithms. Unfortunately, these methods often leak [1], [2] into the parenchyma due to emphysema-related wall thinning or partial volume effects that blur the airway walls. Furthermore, they often fail to detect smaller airway structures and do not provide a complete segmentation in the presence of airway obstruction. Alternative methods such as scale-space particle systems [3] sample the entire search space, thus allowing an efficient comprehensive search in the entire lung.

Lo *et al.* [4] used local image descriptors to model airway appearance as input for subsequent segmentation. Unlike this work, the objective of this study is to present an airway posterior probability model integrating the information of the feature space. The outcome of such model is a probabilistic map that would be useful to optimize the cost function for region growing or fast marching-based segmentation algorithms, and provide morphological clues for an efficient sampling of the image space.

The manuscript is organized as follows: In Section 2, we describe the airway image features and the probability model. In Section 3, we describe the experiment carried out to verify the model proposed. In Section 4, we present the results of the experiment. In Section 5, we discuss the challenges and future extensions.

2. AIRWAY MODEL

2.1. Airway Features

In CT images, lung airways display characteristic features. For instance, it is often observed that the airways are found next to vessels running in a parallel direction [1]. In addition, we formalize other features that characterize airways as follows: (1) airway lumens are dark elongated tubular structures, and (2) airways comprise of a lumen surrounded by an airway wall.

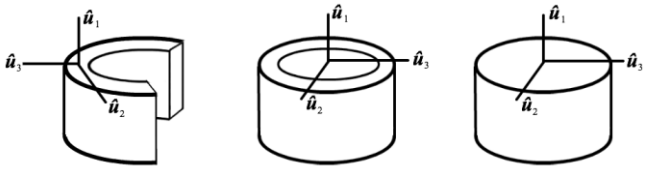

Fig. 1 Principal directions of the Hessian of various structures: (left) wall, (center) airway, and (right) vessel.

The eigenvalue analysis of the Hessian matrix has been proposed to detect various image features [5]. The magnitude, sign and relative values of the eigenvalues λ_k (k=1,2,3) corresponding to the k^{th} normalized eigenvector $\hat{\mathbf{u}}_k$, ordered such that $|\lambda_1|\leq|\lambda_2|\leq|\lambda_3|$, give clues as to the type of underlying structure (see Fig. 1). In this paper we have used combinations of these eigenvalues to derive local operators that produce maximal response for vessels, airways and airway wall voxels, as summarized in Table 1.

All Hessian matrix-based features were calculated at four different scales using Gaussian function with standard deviation σ ranging from 0.5 to 2.0 mm. For each feature, the value taken is the maximum response across the scales.

	λ_1	λ_2	λ_3
Bright tube (e.g. vessels)	Low ≈ 0	High-	High-
Dark tube (e.g. airways)	Low ≈ 0	High+	High+
Bright sheet-like (e.g. airway walls)	Low ≈ 0	Low	High-

Table 1. Possible structure patterns given combination of the Hessian eigenvalues λ_k in 3D images.

Using prior knowledge about the lung anatomy, we can define the following features for each voxel x:

1. Intensity: Intensity $I(x)$ is the voxel value in Hounsfield units (HU).
2. Vesselness and airwayness: Vesselness $V(x)$ is computed using Frangi's filter [5]. Somewhat similar to vesselness, airwayness $A(x)$ is a measure that selects voxels whose combination of eigenvalues is given as defined in the second row of Table 1.

$$A(x)=\begin{cases}0 & \lambda_2<0 \; or \; \lambda_3<0\\ \left(1-exp\left(-\frac{R_a^2}{2\alpha^2}\right)\right)\cdot exp\left(-\frac{R_b^2}{2\beta^2}\right)\cdot\left(1-exp\left(-\frac{S^2}{2c^2}\right)\right) & otherwise\end{cases} \quad (1)$$

where $R_a=\frac{|\lambda_2|}{|\lambda_3|}, R_b=\frac{|\lambda_1|}{\sqrt{|\lambda_2\lambda_3|}}, S=\sqrt{{\lambda_2}^2+{\lambda_3}^2}$

and α, β, and c are parameters that control the sensitivity of the ratios, set at 0.5, 0.5, and 70, as suggested in [5].

3. Wallness: Wallness $W(x)$ detects structures with a change in the direction of the highest curvature. We define a novel measure that computes the normalized Laplacian, $\mathcal{L}$, of the mode of the Hessian $\mathcal{H}$ [6] in the highest curvature direction ($\hat{\mathbf{u}}_3$) modulated by the mode itself, as given by

$$W(x)=\begin{cases}0 & mode\left(\mathcal{H}(x)\right)<0\\ \left|mode\left(\mathcal{H}(x)\right)\right|^2\cdot\frac{\mathcal{L}\left(mode\left(\mathcal{H}(x)\right)\right)}{\left|\mathcal{L}\left(mode\left(\mathcal{H}(x)\right)\right)\right|}\cdot\hat{\mathbf{u}}_3 & otherwise\end{cases} \quad (2)$$

The Laplacian compensates the response of the mode of the Hessian around the wall boundaries to give a strong response at the wall center.

4. Distances to vessels, airways and bronchial walls: Histogram equalization was performed on each of the computed features in order to have an equal distribution of the responses at a certain threshold. Only voxels with post-equalization value > 0.5 were considered to be vessels, airways and bronchial walls, respectively. For each voxel, the distances to the vessels $D_v(x)$, airways $D_a(x)$ and bronchial walls $D_w(x)$ were then computed using Euclidean distance transform.

2.2. Probability Model

The posterior probability $P(A|\hat{\mathbf{X}})$ of those voxels being airway voxels given the feature matrix $\hat{\mathbf{X}}$, was estimated using the well-known Bayes' theorem

$$P(A|\hat{\mathbf{X}})=\frac{P_l(\hat{\mathbf{X}}|A)\cdot P_a(A)}{P_{total}} \quad (3)$$

where $P_{total}=P_l(\hat{\mathbf{X}}|A)\cdot P_a(A)+P_l(\hat{\mathbf{X}}|\bar{A})\cdot P_a(\bar{A})$.

A similar expression can be derived for the non-airway class $\bar{A}$. The *a priori* probabilities of being airway $P_a(A)$ and non-airway $P_a(\bar{A})$ are simply taken as the fraction of airway voxels and non-airway voxels with respect to the total voxel count in the reference data, respectively.

The likelihood of airway $P_l(\hat{\mathbf{X}}|A)$ and non-airway $P_l(\hat{\mathbf{X}}|\bar{A})$ for the feature space $\hat{\mathbf{X}}$ was modeled using a single multivariate Gaussian distribution and a nonparametric kernel density estimation technique based on non-linear principal component analysis (PCA) [7].

The probability distribution function of the Gaussian model is given by

$$P_l(\hat{\boldsymbol{X}})\sim\mathcal{N}(\hat{\mathbf{X}}|\boldsymbol{\mu},\Sigma)=\frac{1}{2\pi^{D/2}|\Sigma|^{1/2}}\cdot e^{\left\{-\frac{1}{2}(\hat{\mathbf{X}}-\mu)^T\Sigma^{-1}(\hat{\mathbf{X}}-\mu)\right\}} \quad (4)$$

where $\boldsymbol{\mu}$ is the D-dimensional mean of the feature matrix $\hat{\mathbf{X}}$, Σ is the covariance matrix, and |Σ| is the determinant of Σ.

The likelihood computed by the kernel density estimation method is defined as

$$P_l(\hat{\boldsymbol{X}})=\mathbf{1}_N^T*\mathbf{U}*\mathbf{U}'*\mathbf{K}(\hat{\mathbf{X}},\hat{\mathbf{Y}}) \quad (5)$$

where $\mathbf{U}$ is the eigenvector matrix of the kernel matrix $\mathbf{K}(\hat{\mathbf{Y}},\hat{\mathbf{Y}})$ for the training data vector $\hat{\mathbf{Y}}$. The kernel is chosen to be a Gaussian, $K(x,y)=e^{-\frac{\|x-y\|^2}{2\sigma^2}}$. For $\mathbf{N}$ testing data points in $\hat{\mathbf{X}}$, $\mathbf{1}_N^T$ is a 1×N column matrix of ones.

3. EXPERIMENTAL PROCEDURE

To verify the airway model proposed, we analyzed 20 CT images from patients enrolled in the COPDGene Program (www.copdgene.org), a multicenter study of genetic and epidemiologic risk factors associated with COPD. Four images were of healthy subjects and the rest were evenly chosen from each Global Initiative for COPD (GOLD) (www.goldcopd.com) stage 1-4. The images were taken with different scanners using the COPDGene acquisition protocol.

3.1. Reference Construction

The reference was constructed from a conservative segmentation of the left and right airway trees using a fast marching algorithm, seeded at the trachea. Arrival time was thresholded initially at 100, gradually increased until leakage (voxel count increase > 100%) occurred, upon which the previous value was taken as the stopping time.

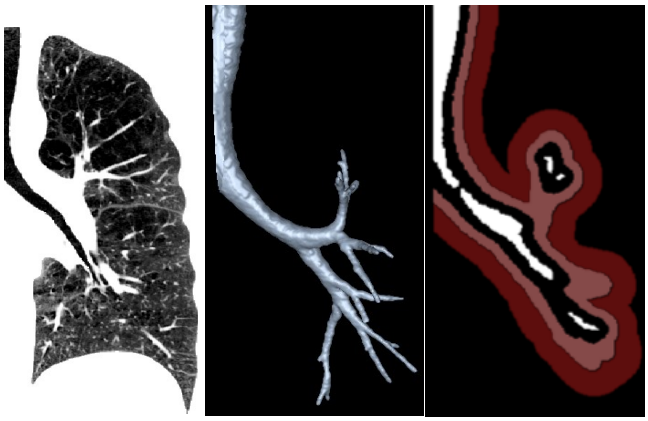

Fig. 2. (left) 2D coronal slice from the original CT; (center) 3D rendering of the conservative segmentation by fast marching; (right) Three labeled zones: AIRWAY zone in white, NON-AIRWAY$_{close}$ zone in pink and NON-AIRWAY$_{far}$ zone in red.

The centerline was calculated using 3D binary thinning of the fully-grown tree. Voxels in the centerline, as well as those within the one-pixel dilate threshold, were labeled AIRWAY. Voxels in the zone between 5 to 10mm from the airway tree were labeled NON-AIRWAY$_{close}$. All voxels from 10 to 20mm outside this zone were given the label NON-AIRWAY$_{far}$. The feature matrix $\hat{\mathbf{X}}$ was calculated for all voxels in each group label. Fig. 2 illustrates a slice of the original CT, the conservative airway tree and the three labeled zones.

3.2. Training and Cross-validation

The feature extraction method described in Section 2 was implemented using InsightToolkit and UNU (Utah Nrrd Utilities). Images of the left and the right lung were trained separately. Two classes were defined: the airway class (C_A), and the combined close and far non-airway classes (C_{NA}). Features from each class were normalized and scaled using the mean and standard deviation. Each class was then downsampled –to limit each class of every image to a manageable maximum of 5000 points– before calculating the posterior probability. Training and 5-fold cross-validation were performed in `matlab` (Mathworks, Natick, MA, US) to test the performance of our posterior probability. Specificity (Sp.) and sensitivity (Sens.) were computed using a maximum a posteriori probability (MAP) classifier criterion. In addition, the medians of the histogram for the posterior probabilities in the testing set were computed for both airway and non-airway classes.

3.3. Feature Selection

We trained and cross-validated separately the Gaussian and nonparametric models, using (1) *all* the features, and (2) an exhaustively determined optimal combination of features for each model. The minimum distance to the perfect classifier *(0,1)* (AC_d) was used to rank the combinations, maximizing sensitivity over specificity. The optimal combinations for the Gaussian and the nonparametric likelihood models are $[A(x),\ D_v(x),\ D_w(x),\ D_a(x),\ I(x)]$, and $[A(x),\ D_v(x),\ D_a(x),\ I(x)]$, respectively.

4. RESULTS

Cross-validation results for feature spaces of airway class $\hat{\mathbf{X}}(C_A)$ and non-airway class $\hat{\mathbf{X}}(C_{NA})$ are given in Table 2. The results reveal that feature selection is important in the Gaussian model but did not greatly improve the nonparametric method. Fig. 3 shows the histograms of two posterior probabilities $P(A|\hat{\mathbf{X}}(C_{NA}))$ and $P(A|\hat{\mathbf{X}}(C_A))$, computed using nonparametric method. While for both models, these histograms have single modes at 0 and 1; the descent in the histogram peak is steeper in the Gaussian model (data not shown), as suggested by the histogram median values M_A and M_{NA} given in Table 2.

Feature space	M_A	M_{NA}	Sp.	Sens.	AC_d
Gaussian					
All features	0.98	0.01	0.56	0.94	0.44
Optimal set	0.90	0.04	0.84	0.85	**0.22**
Nonparametric					
All features	0.78	0.11	0.74	0.91	0.28
Optimal set	0.80	0.10	0.88	0.83	**0.21**

Table 2. Cross validation results for C_A and C_{NA} using both models. M_A and M_{NA} refer to median of histogram of posterior probabilities $P(A|\hat{\mathbf{X}}(C_A))$ and $P(A|\hat{\mathbf{X}}(C_{NA}))$.

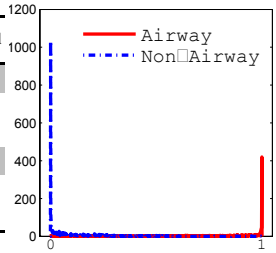

Fig. 3. Histograms of the posterior probabilities $P(A|\hat{\mathbf{X}}(C_A))$ and $P(A|\hat{\mathbf{X}}(C_{NA}))$ as calculated by the nonparametric method.

Table 3 shows the results of analyzing the performance of the classifier trained with features only from subjects within the same GOLD stage. For the Gaussian model, increasing severity of COPD in the training data increases specificity and lowers sensitivity, as shown in Fig 3. In both models, using the healthy group as training data obtained the best performance. Using subjects with GOLD Stage 1 as training data produced worst performance, possibly due to inflammation process often observed at the onset of COPD.

Training Data	M_A	M_{NA}	Sp.	Sens.	AC_d
Gaussian					
Healthy	0.97	0.01	0.81	0.85	**0.24**
GOLD1	0.99	0.00	0.70	0.89	0.32
GOLD2	0.96	0.01	0.78	0.87	0.26
GOLD3	0.93	0.02	0.87	0.78	0.26
GOLD4	0.94	0.02	0.90	0.77	0.25
Nonparametric Method					
Healthy	0.88	0.04	0.88	0.85	**0.19**
GOLD1	0.96	0.02	0.75	0.91	0.27
GOLD2	0.83	0.07	0.85	0.81	0.24
GOLD3	0.83	0.07	0.85	0.85	0.21
GOLD4	0.87	0.06	0.86	0.85	0.21

Table 3. Computed prior probabilities $P(A|\hat{\mathbf{X}}(C_A))$ and $P(A|\hat{\mathbf{X}}(C_{NA}))$ using each GOLD stage as training data.

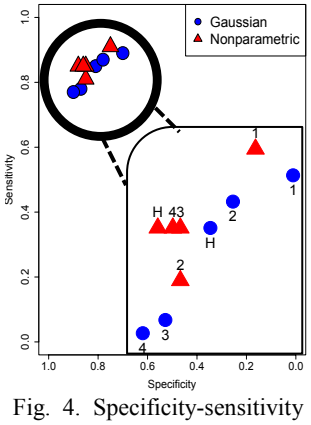

Fig. 4. Specificity-sensitivity plot of classifier trained with only healthy (H) and GOLD stages (1-4) subjects.

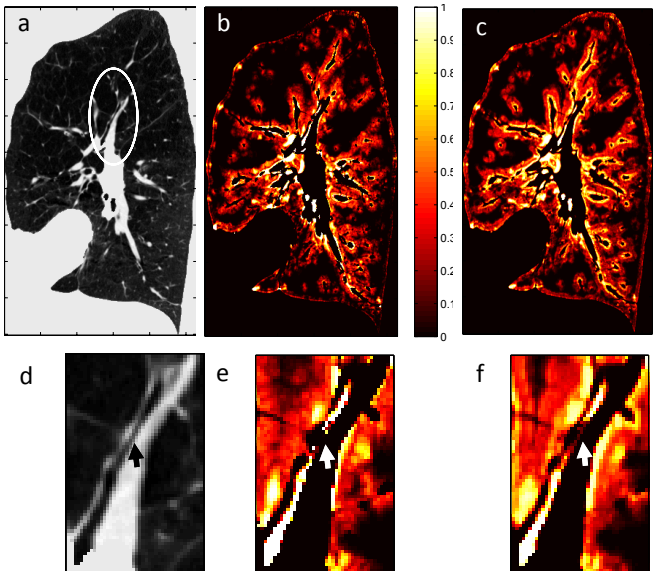

Fig 5. (a) Sample CT slice showing a thin airway (marked with an ellipse). (b-c) Probabilistic images computed by the Gaussian model and the nonparametric method using their respective optimal feature sets. (d) Magnified image of the airway in (a). (e-f) Magnified images of the probabilities computed by the Gaussian model and the nonparametric method.

The posterior probability maps obtained for a sample CT slice are shown in Fig. 5. The images obtained are noisy, although they provide a good indication of the location of the airways. Some regions of the lungs affected by emphysema as well as vessel borders and lung borders have high probability. Interestingly, the probability for a small airway such as the one shown in Fig 5 (d) quickly goes to zero in the Gaussian model, producing discontinuity, while the nonparametric method assigns non-zero values.

Finally, Fig. 6 shows the normalized values of individual features for those voxels with posterior probability higher than 0.9 and lower than 0.1. The features that best distinguish both groups are those in the optimal feature set.

5. DISCUSSION

In this paper, we present an approach to compute the posterior probability of airways based on local features extracted from CT images of the lungs. Amongst the features proposed here is a novel multi-scale wallness measure to detect bronchial wall. The posterior probability has been computed by fitting to the training data two likelihood models: a simple Gaussian distribution and the nonparametric kernel density estimation based on kernel PCA.

The nonparametric method outperformed the Gaussian model, but not dramatically. Optimizing the set of features significantly improved the specificity of the Gaussian model, which was not observed using the nonparametric method. This suggests the nonparametric model is more resilient towards inclusion of less relevant features.

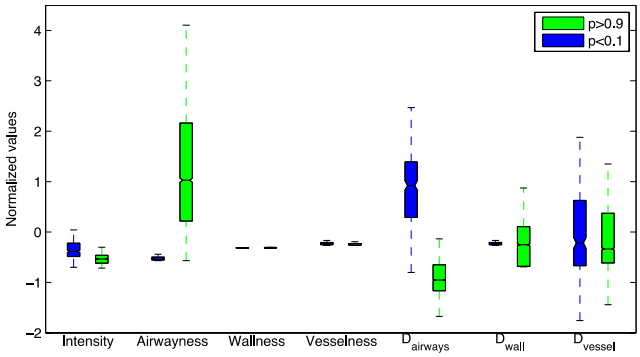

Fig. 6. Normalized values of each feature for voxels with high and low evaluated posterior probability of being airways.

Somewhat unexpected was the exclusion of distance to wall from the set of optimal features for the nonparametric model. It could be due to the noisy wallness measure. Its refinement will be the scope for further study. The use of more sophisticated machine learning methods, such as boosting, may also help us to identify informative features in the automatic feature selection.

Here, we have used naïve *a priori* probability using the ratio of the number of samples in the class and the total number of samples. Results may be improved by leveraging an airway atlas as prior probability. This highlights the flexibility of our approach to include additional information.

Analysis by GOLD stages yields an interesting result: the optimal set of features serves as a stable airway descriptor despite the severity of COPD.

In conclusion, the computed airway probability map integrates valuable information of the feature space and can be used as prior for many segmentation schemes that depend on cost functions.

ACKNOWLEDGEMENT

This project was partially funded by the "UTE Project CIMA", MICINN DPI2009-14115-C03-03, MINECO DPI2012-38090-C03-02 and NIH 1R01HL116931-01. RSJE was funded by NIH NHLBI K25 HL104085.

REFERENCES

[1] Sonka, M. et al., "Rule-based detection of intrathoracic airway trees," IEEE Trans Med Imaging, vol. 15, no. 3, pp. 314–26, 1996.

[2] Tschirren, J. et al., "Segmentation and quantitative analysis of intrathoracic airway trees from computed tomography images," Proc Am Thorac Soc, vol. 2, no. 6, pp. 484–7, 503–4, 2005.

[3] Kindlmann, G. L. et al., "Sampling and visualizing creases with scale-space particles.," IEEE Trans Vis Comput Graph, vol. 15, no. 6, pp. 1415–24, 2009.

[4] Lo, P. et al., "Vessel-guided airway tree segmentation: A voxel classification approach," Med Image Anal, vol. 14, no. 4, pp. 527–538, 2010.

[5] Frangi, A. F. et al., "Multiscale vessel enhancement filtering," in *Medical Image Computing and Computer-Assisted Intervention*, vol. 1496, 1998, pp. 130–137.

[6] Ennis, D. B., Kindlmann, G., "Orthogonal tensor invariants and the analysis of diffusion tensor magnetic resonance images.," Magn Reson Med, vol. 55, no. 1, pp. 136–46, 2006.

[7] Schölkopf, B. et al., "Nonlinear Component Analysis as a Kernel Eigenvalue Problem," Neural Comput, vol. 10, no. 5, pp. 1299–1319, 1998.